

Solidification behaviour in plasma arc welding

G RAVICHANDRAN

Welding Research Institute, BHEL, Tiruchirappalli 620 014, India
e-mail: drgravi@yahoo.com; WRI_Purchase (wri@bheltry.co.in)

Abstract. Melting and solidification behaviour in the deep penetration welding process is different from that in conventional welding processes. In deep penetration processes, there is keyhole formation and the full thickness of the plate receives the arc heat input unlike in conventional processes in which the heat input is received only by the surface nodes. In the present study, the thermal analysis of molten pool formation and solidification for keyhole welding using plasma arc welding has been done using the finite element method. The model accounts for the several phenomena associated with welding, like the distributed arc heat input over the top surface and along the thickness, the temperature-dependent material properties, convection and radiation heat losses etc. The analysis is performed for different combinations of parameters, viz. welding current and welding speed, which have the maximum influence on molten pool shape and solidification behaviour. The model has also been validated by conducting experimental measurement of thermal cycles experienced by the plate for different welding parameters. The weld pool dimensions, viz. the length and width are found to increase with increasing current and decreasing welding speed. Thermal cycles at locations close to the weld reach a higher value of temperature and the time for peak temperature is also less but at farther locations, the peak temperature reached is lower and the time for peak temperature is higher. Details of the model, the experimental results obtained and the solidification characteristics of the pool are discussed in this paper.

Keywords. Plasma arc welding; keyhole technique; finite element model; transient thermal analysis; solidification behaviour; welding parameters.

1. Introduction

Welding is one of the most popular techniques for the manufacture of engineering structures as it has several advantages over other techniques. With the rapid advances in technology in core sectors like nuclear, aerospace, defence and power, engineering components and structures are required to perform satisfactorily under different operating conditions. Newer materials are being developed for these special applications and tested for their weldability characteristics. Quite often, getting radiographic quality joints in these materials with conventional welding processes is difficult. Hence in the last three decades,

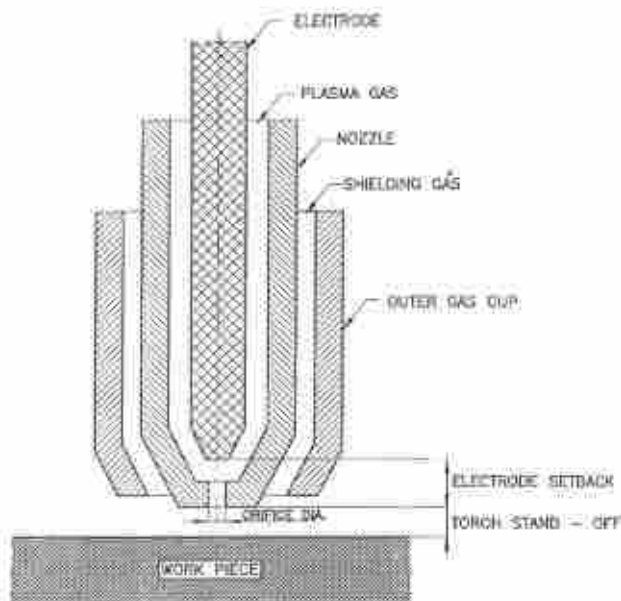


Figure 1. Plasma arc welding torch terminology.

newer welding processes and techniques have been developed and employed to meet the stringent quality requirements. These advanced welding techniques, like plasma arc welding, electron beam welding and laser beam welding, employ high power densities in the weld region, of the order of 10^7 to 10^{12} W/m², compared to those, of the order of 10^4 to 10^5 W/m², in other conventional arc welding processes. Due to the high power densities employed, deep penetration is achieved in the material being welded, and thus the quality of the weld joint is very good.

The plasma welding process uses the energy produced by the arc generated between a non-consumable electrode and the base metal. The arc is physically constricted by means of a copper nozzle having a small orifice at the centre as shown in figure 1. An inert gas is continuously fed into the arc chamber and gets ionised as it passes through the gap between the electrode and the nozzle. Due to this constriction, the current density in the arc is much higher and the high temperature arc column comes out at high velocity. This high velocity high temperature plasma is utilised for a variety of applications such as welding, cutting, surfacing and spraying. For welding purposes, the keyhole technique is popularly employed and a schematic sketch illustrating the technique is shown in figure 2. The keyhole effect lies in the transition phase between melt-in mode and cutting mode. In the melt-in mode, the arc creates a molten pool and by and large does not displace it. In the cutting mode, the molten metal is created and ejected out of the joint location forcibly. In the keyhole action, the arc creates the molten pool upto the bottom layer and temporarily displaces it to the rear. The keyhole action depends on the characteristics of the welding arc, such as temperature, velocity, and density of the plasma, which are governed by the energy input and the arc constriction.

When welding commences on the new plate, due to the deep penetrating plasma arc column, a hole is created throughout the thickness of the joint and as the hole traverses, the molten metal flows around the keyhole to the rear and gets solidified to form the weld. The keyhole produced in plasma welding mainly depends on the arc current, speed of welding, plasma gas flow rate, thickness of the joint and physical parameters of the material being

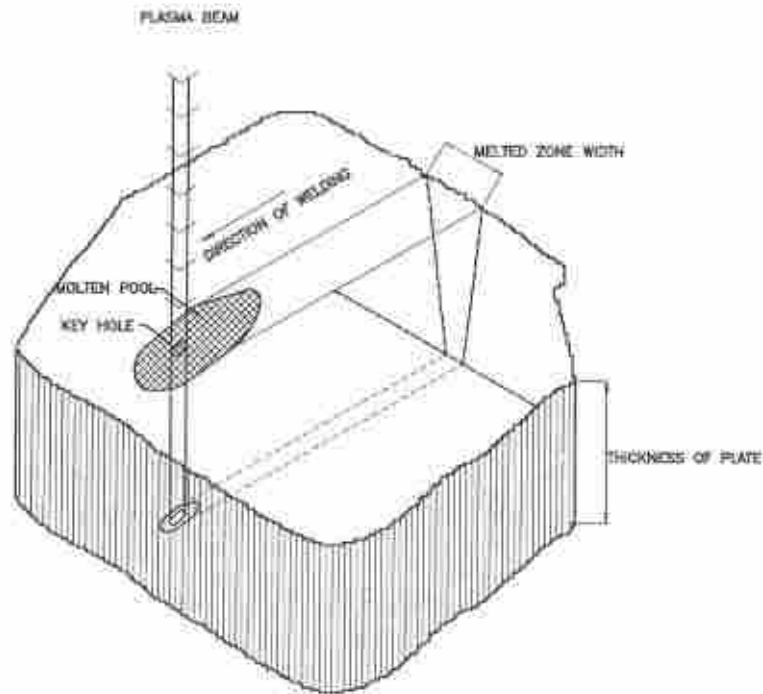


Figure 2. Keyhole effect in deep penetration welding.

welded. The operating weld parameter window required to form a keyhole is usually a narrow zone and the parameters have to be kept within this narrow window throughout the weld. The stability of the keyhole can be understood by the assessment of the forces which exist at the bottom of the plate where the effluent plasma emerges. The keyhole is sustained by the resultant action of the various forces which include plasma gas pressure, welding parameters, surface tension of the liquid metal and backing gas pressure. Keyhole welding is generally possible for the thickness range between 2.5 and 7 mm for stainless steels. The associated advantages with this technique include higher speed of welding, consistent quality of the weldment, lower residual stresses and distortion and amenability for mechanisation.

Temperature distribution and thermal cycles during welding using transient thermal analysis have been studied by various researchers to determine the effect of operating parameters on the melting and solidification behaviour of the metal. The study of thermal cycles in a weldment is required for the analyses of various phenomena like distortion and build-up of residual stresses, microstructure at different zones of the weld, hydrogen diffusion in the weld metal, cold cracking susceptibility of the weld metal etc. The initial researchers employed the analytical solution for the heat flow in welding using a quasi-stationary model, which is applicable when the arc is moving at constant speed and the end effects are neglected. The quasi-stationary model assumes a moving coordinate system with the origin at the centre of the arc, and in this moving coordinate system, temperature distribution in the plate becomes stationary. Hence, the three-dimensional problem reduces to a two-dimensional model for a section perpendicular to the weld line. However, with development in computing power and numerical techniques like the finite element method, which can represent many phenomena associated with welding,

full three-dimensional models are popularly employed for transient thermal analysis. With these three-dimensional models, there is no need for any limiting assumptions and the model can predict the thermal results at all the locations accurately.

The study of heat transfer in high energy density processes is different from the conventional processes, as in the high energy density processes, heat is input along the full thickness of the plate unlike in the case of conventional processes. The modelling of arc heating as a point source or line source idealises a heat source, which in reality is distributed. This assumption of point or line source gives results which are accurate at locations far from the heat source, but at the source the error in temperature is large – sometimes even infinite. However, initial researchers (Swiftbook & Gick 1973) assumed linear energy distribution in the thickness direction for simplifying the complex problem. Subsequent researchers (Mazumder & Steen 1980; Giedt 1986) studied the keyhole welding in high energy density processes like electron beam welding and laser welding using some distribution function for the heat source. With these models, the depth of penetration, temperature variation within the liquid surface of the cavity and the dimensions of the cavity were predicted. Unlike earlier, the material properties were assumed to be a function of temperature in the latter models (Tekriwal *et al.* 1987), which also improved the accuracy of the model.

With the development in high performance computing of over one billion floating point operations per second (Zacharia *et al.* 1993) supercomputers provide exciting new opportunities for process modelling by allowing the implementation of more complex databases and realistic simulations. The modelling of welding processes provides good examples of situations where descriptions of turbulence, multiphase flow, electromagnetic and surface tension flow, transient heat transfer and evaporation can be used to characterise complex physical phenomena. Newer techniques such as geometric constraint method are devised (Lambrakos 1995) to account for the constraints based on boundary information obtained from experiments so that the simulation of deep penetration welding can be more effective.

The objective of the present work is to study the melting and solidification mechanism of a plasma arc welded plate using finite element analysis. The transient thermal analysis is conducted using three-dimensional brick elements and the arc heat input is assumed to be distributed in the lateral directions as well as in the thickness direction. Temperature dependency of the material properties and the heat losses due to convection and radiation are also included in the model. The analysis is used for the determination of the molten pool size and the thermal cycles in points adjacent to the weld through the analysis of the molten zone isotherms.

2. Finite element model

The governing equation for the transient heat transfer equation in the finite element method is written as,

$$[C]\{\partial T/\partial t\} + [K]\{T\} = \{F\},$$

where $[C]$ is the thermal capacitance matrix given by

$$\int_{\Omega} \rho C_p [N]^T \cdot [N] dV,$$

$[K]$ is the thermal conductance matrix given by

$$\int [B]^T \cdot [D] \cdot [B] dV + \int h_0 [N]^T \cdot [N] dS.$$

$[F]$ is the thermal load vector given by

$$\int q \cdot [N]^T dS + \int h_0 \cdot T_\infty \cdot [N]^T \cdot dS.$$

$[N]$ is the shape function matrix, $[B]$ is the derivative of shape function matrix, $[D]$ is the matrix containing thermal conductivities, T is the temperature in $^{\circ}\text{C}$, ρ is the density of the material in kg/mm^3 , C_p is the specific heat in $\text{J}/\text{kg } ^{\circ}\text{C}$, h_0 is the overall heat loss parameter in $\text{W}/\text{mm}^2\text{ } ^{\circ}\text{C}$ (explained below), T_∞ is the ambient temperature in $^{\circ}\text{C}$, q is the arc heat flux in W/mm^2 , V is the volume, S is the surface area, t is the time.

The plate taken for transient analysis has dimensions of $180 \times 150 \times 6.7$ mm and the material of the plate is AISI 304 grade stainless steel. The plasma arc welding is done in the centre of the plate without any filler addition which represents butt welding of two plates held with zero root gap. Due to symmetry, only one half of the plate is taken for the analysis. The plate is discretised into a number of eight-noded brick elements as shown in figure 3. The elements are of smaller size in places close to the weld as the temperature gradients are expected to be steep in these locations and at further locations the size is progressively increased. There are 5 nodes in the thickness direction at equal distances. The total number of nodes and elements are 4550 and 3240 respectively.

For each of the elements, the elemental $[k]$ and $[c]$ matrices are computed using the equation given above. For computation of the two matrices, the temperature dependence of the material properties, viz. thermal conductivity and specific heat, is required. For AISI 304 grade stainless steel, variations of thermal conductivity and specific heat are assumed as given by Tekriwal *et al* (1987) and are shown in figure 4. Thermal conductivity increases with temperature until the boiling point is reached. Once temperature rises beyond the boiling point of the material, thermal conductivity is reduced to a low value, as then the conductivity corresponds to that of the metallic vapour only. However, in the molten condition, the high value of thermal conductivity is retained as even though the thermal conductivity of liquid metal is lower, the convective heat transfer due to the stirring of the molten pool is higher and has to be taken into account. Similar variation is assumed for the specific heat of the material. The density of the material also varies with temperature but the variation is neglected in this analysis.

For computation of the arc heat flux, the efficiency of the welding process has to be determined. The efficiency corresponds to the amount of heat which is effectively transferred to the base metal. The efficiency of plasma welding is calculated using three

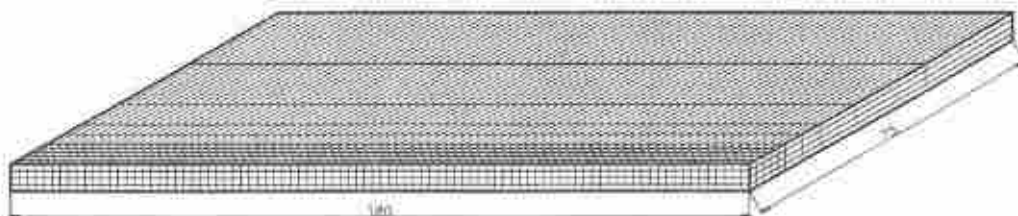


Figure 3. Discretisation of the plate for the analysis.

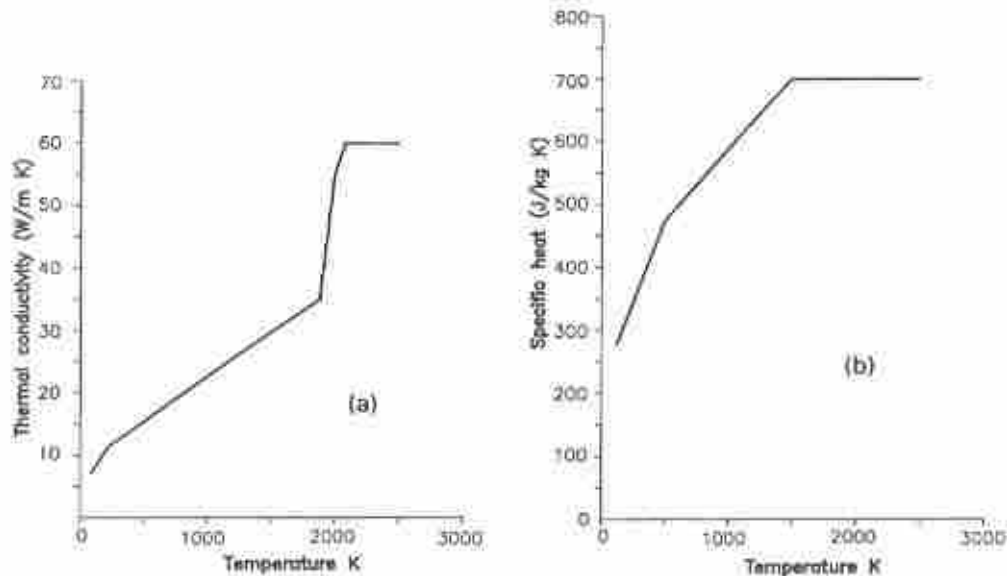


Figure 4. Variation of (a) thermal conductivity, and (b) specific heat, with temperature (Tekriwal *et al.* 1987).

sources of heat input viz. anodic heating, radiation of heat from plasma and convective heat transfer from plasma to the metal. In conventional processes, anodic heating is most significant whereas in plasma welding, the most significant contribution comes from convective heat transfer followed by anodic heating and radiation heat transfer. Metcalfe & Quigley (1975) have evaluated the efficiency in plasma welding as 0.64 for the keyhole process and 0.68 for the melt-in mode of the plasma welding process. The efficiency in the keyhole process is lower due to the fact that the effluent plasma gas carries away some part of the heat but in the melt-in mode, the top layer receives the heat and the loss of heat due to effluent plasma is not present.

The arc heat flux varies in the two dimensional plane across the arc and researchers like Friedman (1975) and Krutz & Segerlind (1978), have assumed Gaussian distribution for the arc heat. This distribution assumes that 95% of the arc heat energy falls within a circle of given radius, and inside the circle the energy changes exponentially from the centre to the end. Other researchers like Goldak *et al.* (1986) have assumed a more correct double ellipsoidal heat flux model but in this present model only the Gaussian energy distribution is assumed for the arc heat in the two dimensional plane across the arc. The radius of the arc is taken to be 4 mm at the top and tapers to 1 mm at the bottom. When the plasma column impinges on the material, it results in full penetration of the plate, and as the plasma column moves along the plate, the full thickness of the plate receives the heat input. The variation of the heat input along the thickness direction z is taken to be exponential in nature as per the Beer-Lambert law (Mazumder & Steen 1980) as given below.

$$Q_{\text{any depth } z} = q_{\text{surface}} \cdot \exp(-B \cdot z),$$

The value of B is taken to be 0.8 mm^{-1} as given by Mazumder & Steen (1980). Thus the variation of the arc heat flux at any point (x, y, z) from the centre of the arc is given by

$$q = 3 \cdot Q / \pi R^2 \cdot \exp(-3(x^2 + y^2)/R^2) \cdot \exp(-Bz),$$

where q is the heat flux at any point x, y, z lying under the arc in W/mm^2 , Q is the heat input in watts given by ηIV , η is the efficiency of plasma welding process assumed to be 0.64, I is the current in A, V is the voltage in V, R is the radius of the arc in millimetres assumed to be 4 mm, B is the parameter assumed to be 0.8 mm^{-1} , x, y and z are the coordinates from the centre of the arc.

The arc is a moving source of heat and at any point of time, the arc occupies a particular position on the plate. For this position of the arc, the nodes which fall below the arc are noted and the arc heat flux is calculated for these using the relation given above. The arc takes some time for crossing a point depending on its radius and the speed of welding. The heat input increases as the arc approaches the point and is the maximum when the centre of the arc is directly over the point. Thereafter, the heat flux starts falling and once the arc has completely moved over the point, no heat falls on the point any longer.

In the weld pool vicinity, heat is lost to surrounding environment by convection and radiation due to high difference in the surface and ambient temperatures. For determining the heat loss due to radiation, the equivalent heat loss parameter as proposed by Asibu *et al* (1989) which accounts for the convective and radiation heat losses is calculated and applied to all the surface nodes. The equivalent heat loss parameter is calculated as

$$h_0 = h_c + \sigma \epsilon (T_{i-1}^2 + T_\infty^2) \cdot (T_{i-1} + T_\infty),$$

where h_c is the convection coefficient in $\text{W/mm}^2\text{ }^\circ\text{C}$, σ is the Stefan-Boltzmann's constant, ϵ is the emissivity of the surface, T_{i-1} is the temperature corresponding to the previous time step in $^\circ\text{C}$, and T_∞ is the ambient temperature in $^\circ\text{C}$.

The convection heat loss coefficient is taken to be $1.144 \times 10^{-6} \text{ W/mm}^2\text{ }^\circ\text{C}$ for the top surface and $2.288 \times 10^{-6} \text{ W/mm}^2\text{ }^\circ\text{C}$ for the bottom surface. The lower value is assumed for the top surface as this surface is exposed to the hot plasma gases whereas the bottom surface is only exposed to the backing gas. Emissivity value is assumed to be 0.4 for all surface nodes. Latent heat is not included in the analysis as the effect of latent heat is only to shift the molten pool backwards and not cause an increase or decrease in the size of the molten pool dimensions.

After assembling the global $[C]$, $[K]$ and $[F]$ matrices, the solution is obtained in the time domain using Galerkin's scheme of time marching. Goldak *et al* (1986) have given the time discretisation requirements and mentioned that the time step should be so selected that the rise and fall of temperatures at any node for a time interval should not be very steep. In the present model, the arc is assumed to advance by 0.5 mm for each time step and hence the time step during the welding phase is accordingly chosen for the case involving a welding speed. The problem is nonlinear in nature as material properties are functions of temperature and the solution requires many iterations within a time step. The analysis is simplified however as proposed by Asibu *et al* (1989) wherein the temperatures for any time step are obtained by evaluating the thermophysical properties and heat transfer coefficients using thermal results corresponding to the previous time step. With this procedure, the complex scheme of iterating within a time step are avoided and the problem is simplified.

The total number of time steps are 360 for the heating stage when the arc moves from one end to the other end and once the arc has covered the full length of the plate, further heat input is stopped and the plate is allowed to cool down. During the cooling stage, the time steps are progressively increased as the temperature gradient slows down. The analysis is run for another 36 time steps in the cooling phase up to a time of 2000 seconds and by this time the plate gets cooled down significantly. The analysis is performed using a

computer program developed for the purpose using C language and run on a PC with Pentium configuration. After each time step, the program stores the temperature results for all the nodes in a file.

3. Experimental validation

The finite element model has been validated using experimental trials (Ananthan 1989; Ravichandran & Ananthan 1998). As the measurement of temperature in the weld is very difficult, measurements were carried out at distances starting from 6 mm from the centre of the weld. The experimental study for the validation of the model was conducted using Plasma system PK 300 consisting of Thermal Dynamics PWM-4A welding torch, a constant current type of power source and associated control system WC 122, which includes the pilot arc supply, high frequency arc initiator, torch water cooling, and controls for plasma gas and shield gas. The overall view of the welding set-up is shown in figure 5. The trials were conducted on an AISI-304 grade stainless steel plate of size $175 \times 150 \times 6.7$ mm.



Figure 5. Overall view of the experimental set-up.

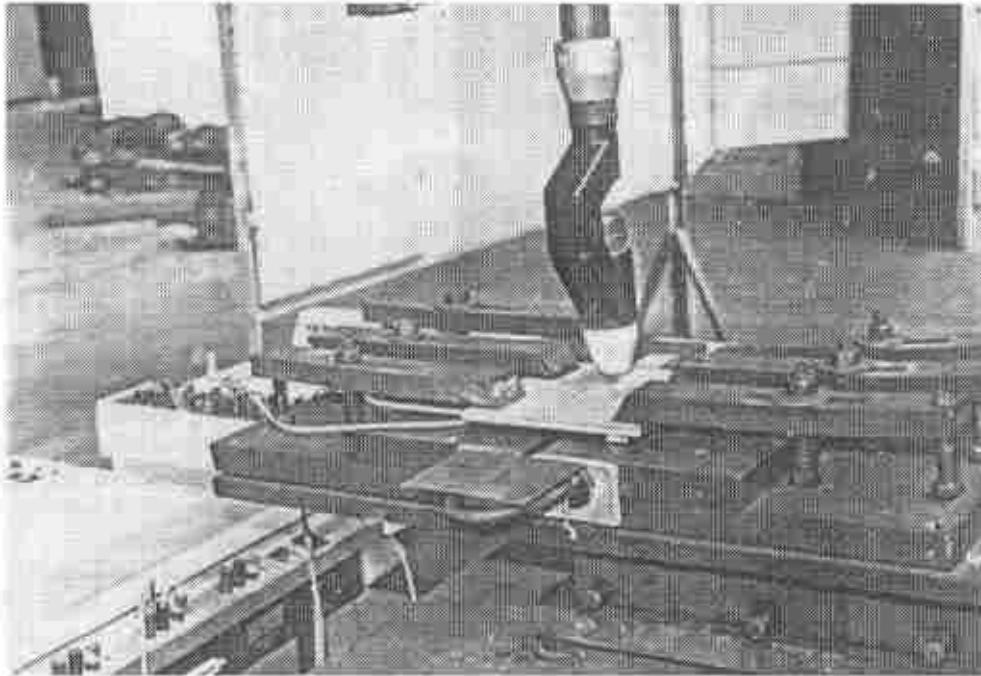


Figure 6. Close-up view of the welding bead and the set-up.

The close-up view of the welding set-up is shown in figure 6. Bead-on-plate welding trials were conducted over the plate as this simulates a butt-weld joint with zero root gap. Temperatures were measured using chromel–alumel thermocouples of diameter 0.8 mm which were fixed on the plate surface using capacitor discharge welding. The thermocouples were fixed at 6, 13 and 20 mm from the weld centre. The plate was clamped on a fixture with provision for back shielding.

The welding trials were carried out at two levels of current (175 A and 210 A) and two levels of welding speed (150 mm/min and 170 mm/min). The arc voltage was kept at 30 V and 31 V for the two current levels. The stand-off distance between the torch and the top surface of the job was kept at 5.5 mm. The flow rates of the plasma gas, the shielding gas and the back-up gas were maintained at 2 lpm, 10 lpm and 5 lpm respectively. These parameters were selected using a scheme of statistical design of experiments. The phenomenon of the keyhole occurs in a narrow range of parameters and the current and welding speed were the predominant factors. Thus the parameters were selected within a short range. The plasma gas and back up gas flow rates which play an important role for the displacement of the liquefied metal has not been varied as this effect has not been included in the model.

4. Results and discussion

The deep penetrating nature of the plasma arc results in complete fusion of the material along the thickness direction but as the power of the arc decreases exponentially in the thickness direction, the extent of fusion will be different for the top and the bottom layers.

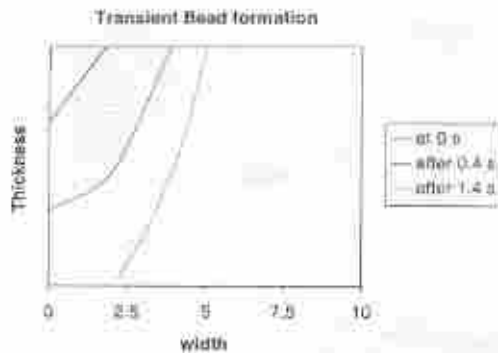


Figure 7. Progressive penetration in the plate due to plasma arc welding.

The top layer which receives the maximum heat input melts almost immediately when the arc covers the point. Due to the progressive heat conduction and digging action of the arc and blowing out of the molten metal, the bottom layer melts after some time lag. The material of the plate, viz. stainless steel, melts over a temperature range of 1400°C to 1450°C but for ease of analysis, the melting is assumed to occur at 1450°C. The progressive penetration of the surface due to the impinging plasma arc is shown in figure 7 for the first case (current 175 A and welding speed 150 mm/min); the results are similar for the other three cases. In all the cases, it was found that the top layer melts to a larger extent and the width of the molten zone is higher at the top than at the bottom. Full penetration is achieved after a time lag of 1.6 s when the centre of the plasma arc moves over the section.

Solidification proceeds in the direction opposite to the melting and proceeds from the bottom to the top. The lower heat input at the bottom surface due to the Beer-Lambert law, higher convection heat losses at the bottom and lower width of the molten pool size at the bottom surface result in solidification commencing at the bottom surface. Solidification begins immediately after the periphery of the arc crosses the point and at the top surface is complete only after 4-6 seconds.

Temperature distribution in the plate when the arc is directly over the point is shown in figure 8 for 175 A current and 150 mm/min welding speed. The temperature distribution shows large difference between the top and the bottom layers up to a distance of about 6-7 mm which is the thickness of the plate. Thereafter, this difference is not significant. The difference is highest at the centre of the weld and, at this point, the top layer is at a high temperature much beyond the boiling point of steel, whereas the bottom layer is just above the melting point. The trend is similar for the other combinations of current and welding speed conditions also.

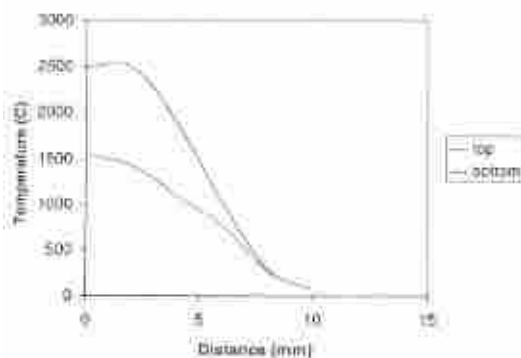


Figure 8. Temperature distribution in the plasma arc welded plate from the weld end.

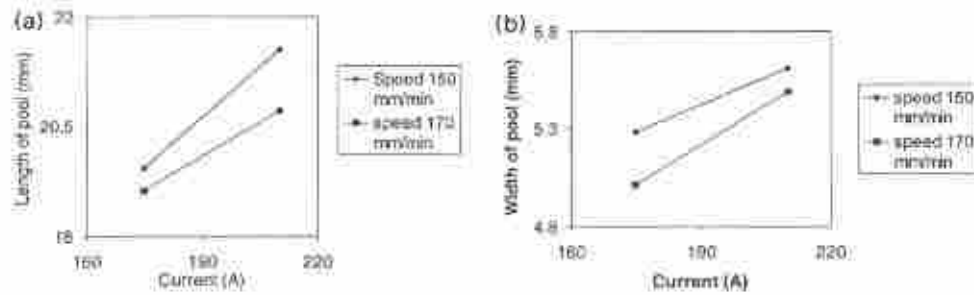


Figure 9. Molten pool dimensions as a function of the weld parameters.

Dimensions of the molten pool, viz. the length and width of the molten pool at the top surface, show variations at different parametric combinations. In the analysis, the parameters could not be varied by a larger extent as attainment of satisfactory keyhole conditions is possible only within a narrow range. However, the trend is clearly seen for this narrow range, as shown in figure 9. Length and width of the pool increase with increase in current. The effect of welding speed is just the opposite and pool dimensions decrease with increase in welding speed. When current is increased, the heat content of the arc and the energy transferred to the plate are higher, which results in higher peak temperature in the molten pool and slower cooling rates. Hence, length and width of the molten pool are higher. When welding speed is increased, the energy is distributed over a longer length and thus heat input at any given section is reduced, which results in just the opposite effect.

Combining the two parameters, welding heat input per unit length, computed as $\eta V/Iv$ where η is the efficiency, V is the voltage, I is the current and v is the welding speed, is calculated and plotted against the molten pool dimensions. From the graph shown in figure 10, it is seen that when the heat input per unit length is increased, the length and width of the molten pool are higher, but the rate of rise is very shallow. For a 36% increase in heat input per unit length, the length and width of the molten pool increase by only 17% and 12% respectively. Among the variables, current has a higher effect on the length and width compared to welding speed. When current is raised by 20%, the length and width

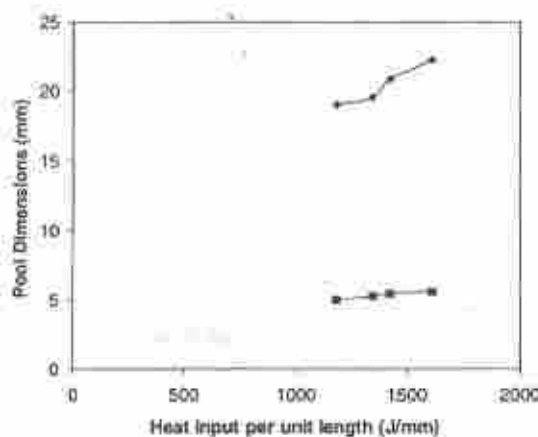


Figure 10. Molten pool dimensions as a function of weld heat input per unit length.

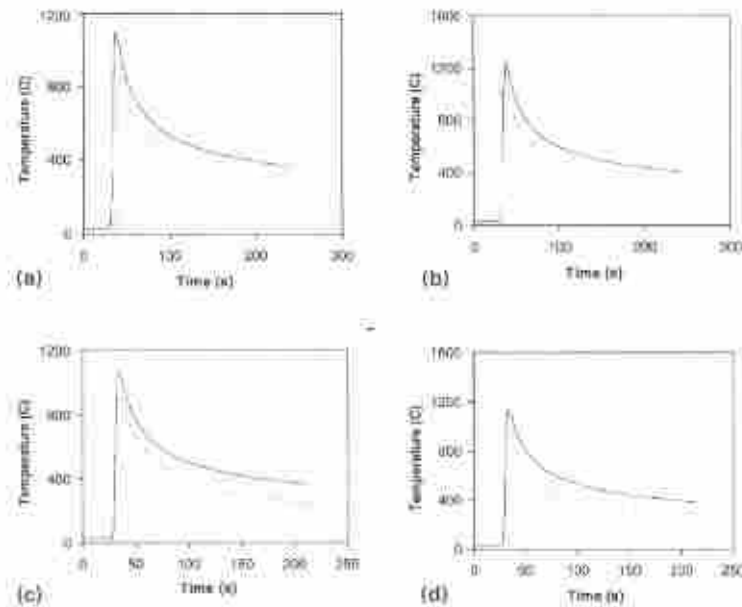


Figure 11. Comparison between computed (—) and experimental (---) thermal cycles at 6 mm distance from the weld line for 4 cases, current and speed respectively being 175 A and 150 mm/min (a), 210 A and 150 mm/min (b), 175 A and 170 mm/min (c), and 210 A and 170 mm/min (d).

increase by 12% and 7.5% respectively, whereas when speed is reduced by 11%, the length and width increase by 4% and 3% only.

Comparison between the theoretical and experimental thermal cycle results for four cases at 6 mm distance from the weld centre is shown in figure 11a to d (Ananthan 1989). Thermal cycles during welding are dependent on the distance from the weld centre. At points close to the weld centre, peak temperatures are higher and the time duration for which the peak temperature is experienced is shorter. But at points well away from the weld centre, peak temperatures are lower and occur after very long time lags. In the present case, at a distance of 6 mm, peak temperatures are high but well within the melting point of the material and the peak temperature also occurs within a short time. As expected, the maximum temperature is experienced for the case with 210 A current and 150 mm/min welding speed, which has the highest heat input per unit length of the weld. Conversely, peak temperature is the lowest in the case of 175 A current and 170 mm/min welding speed. Among the other two cases, peak temperature is higher for 210 A and 170 mm/min welding speed, as the heat input per unit length is higher in this case as compared to the other.

Figures 11a–d show that the agreement between the computed and experimental results is within 15%, with the experimental values being less than the computed ones. The deviations could be due to the higher heat losses than has been accounted in the model and uncertainties in the properties of the material at elevated temperatures. The deviation could also be due to the fact that the physical displacement of the liquid metal is not accounted for in the model. The deviation between computed and experimental values becomes less at other farther locations. However, considering the various limitations, agreement between the two sets of values is reasonably good and thus the finite element model is validated.

5. Conclusions

A finite element method-based transient thermal model has been successfully developed and applied for transient thermal analysis of the deep penetration plasma arc welding process. The various phenomena associated with deep penetration welding, like the distributed arc heat input in the radial direction and thickness direction, temperature-dependent material properties, surface heat losses etc., have been incorporated in the model. The model has been validated through experimental trials involving different parameter combinations with measurement of temperature at different distances from the weld centre. The close results obtained show the efficacy of the model. Thermal results obtained for different parametric combinations show that the welding current influences the solidification profile and the dimensions of the molten pool to a larger extent compared to the welding speed. The thermal cycles between the top and bottom surfaces at the weld centre show large deviation up to a distance equal to about the thickness of the plate, while beyond this distance the deviation is negligible.

References

- Ananthan S S 1989 *A study on the effects of parameters and development of keyhole monitor for plasma keyhole welding*. M S thesis, Indian Institute of Science, Bangalore
- Anbu E K Jr, Kikuchi N, Jaffad A R 1989 Experimental finite element analysis of temperature distribution during arc welding. *Trans. ASME, J. Eng. Mater. Technol.* 111: 9–18
- Friedman E 1975 Thermomechanical analysis of welding process using finite element method. *Trans. ASME J. Pressure Vessel Technol.* 97: 206–213
- Giedt W G 1986 Heat transfer and fluid flow in electron beam welding. *Proc. Conference on Trends in Welding Research in USA* (ed.) S A David (New Orleans, LA: Am. Soc. Metals) pp 109–128
- Goldak J, Bibby M, Moore J, House R, Patel B 1986 Computer modelling of heat flow in welds. *Metal Trans.* B17: 587–600
- Krutz G W, Segerlind L J 1978 Finite element analysis of welded structures. *Welding J.* 57(7): 211s–216s
- Lambrakos S G 1995 Simulation of deep penetration welding of stainless steel using geometric constraints based on experimental information. *Proc. 4th Int. Conf on Trends in Welding Research* (eds) H B Smartt, J A Johnson, S A David, Sponsored by ASM Intl. and Am. Welding Soc., pp 45–50
- Mazumder J, Steen W M 1980 Heat transfer model for CW laser material processing. *J. Appl. Phys.* 51: 941–947
- Metcalfe J C, Quigley M B C 1975 Heat transfer in plasma arc welding. *Welding J.* 54: 99s–103s
- Ravichandran G, Ananthan S S 1998 Analysis of thermal cycles during plasma arc welding by finite element method. *Welding Res. Inst.* 19(2): 57–63
- Swifhook D T, Giek A E F 1973 Penetration welding with lasers. *Welding J.* 52: 492s–499s
- Tekriwal P, Stitt M, Mazumder J 1987 Finite element modeling of heat transfer in gas tungsten arc welding. *Metal Construction* 19: 599–606
- Zacharia T, Bjerke M A, Simutovic S 1993 High performance computing for materials process modeling. *Int. Conf. on Modeling and Control of Joining Processes* (ed.) T Zacharia, cosponsored by American Welding Society and Oak Ridge National Laboratory, pp 27–35